JACS
JOURNAL OF THE AMERICAN CHEMICAL SOCIETY
Article
pubs.acs.org/JACS

Magnetic Resonance Imaging of Tumor with a Self-Traceable Phosphorylcholine Polymer

Hisatsugu Yamada,[†,#] Yoshinori Hasegawa,[‡] Hirohiko Imai,[§,#] Yuki Takayama,[§] Fuminori Sugihara,[§] Tetsuya Matsuda,[§] Hidehito Tochio,[¶] Masahiro Shirakawa,[¶] Shinsuke Sando,[∥] Yu Kimura,[⊥] Akio Toshimitsu,[‡,▽] Yasuhiro Aoyama,*[,○] and Teruyuki Kondo*[,†,‡]

[†]Advanced Biomedical Engineering Research Unit, Center for the Promotion of Interdisciplinary Education and Research, Kyoto University, Katsura, Nishikyo-ku, Kyoto 615-8510, Japan

[‡]Department of Energy and Hydrocarbon Chemistry, Graduate School of Engineering, Kyoto University, Katsura, Nishikyo-ku, Kyoto 615-8510, Japan

[§]Department of Systems Science, Graduate School of Informatics, Kyoto University, Yoshida-honmachi, Sakyo-ku, Kyoto 606-8501, Japan

[¶]Department of Molecular Engineering, Graduate School of Engineering, Kyoto University, Katsura, Nishikyo-ku, Kyoto 615-8510, Japan

[∥]Department of Chemistry & Biotechnology, School of Engineering, The University of Tokyo, 7-3-1 Hongo, Bunkyo-ku, Tokyo 113-8656, Japan

[⊥]Research and Educational Unit of Leaders for Integrated Medical System, Center for the Promotion of Interdisciplinary Education and Research, Kyoto University, Katsura, Nishikyo-ku, Kyoto 615-8510, Japan

[▽]Division of Multidisciplinary Chemistry, Institute for Chemical Research, Kyoto University, Gokanosho, Uji, Kyoto 611-0011, Japan

[○]Kyoto University, Katsura, Nishikyo-ku, Kyoto 615-8510, Japan

Supporting Information

ABSTRACT: Polymers are concentration-amplified with respect to the monomeric units. We show here that a phosphorylcholine polymer enriched with $^{13}C/^{15}N$ at the methyl groups is self-traceable by multiple-resonance (heteronuclear-correlation) NMR in tumor-bearing mice inoculated with the mouse rectal cancer cell line (colon 26). Preliminary measurements indicated that the present polymeric nanoprobe was satisfactorily distinguished from lipids and detectable with far sub-micromolar spectroscopic and far sub-millimolar imaging sensitivities. Detailed ex vivo and in vivo studies for the tumor-bearing mice administered the probe with a mean molecular weight of 63 000 and a mean size of 13 nm, revealed the following: (1) this probe accumulates in the tumor highly selectively (besides renal excretion) and efficiently (up to 30% of the injected dose), (2) the tumor can thus be clearly in vivo imaged, the lowest clearly imageable dose of the probe being 100 mg/kg or 2.0 mg/20-g mouse, and (3) the competition between renal excretion and tumor accumulation is size-controlled; that is, the larger (higher molecular-weight) and smaller (lower molecular-weight) portions of the probe undergo tumor accumulation and renal excretion, respectively. The observed size dependence suggests that the efficient tumor-targeting of the present probe is stimulated primarily by the so-called enhanced permeability and retention (EPR) effect, that is, size-allowed invasion of the probe into the tumor tissue via defective vascular wall. Self-traceable polymers thus open an important area of magnetic resonance imaging (MRI) of tumors and may provide a highly potential tool to visualize various delivery/localization processes using synthetic polymers.

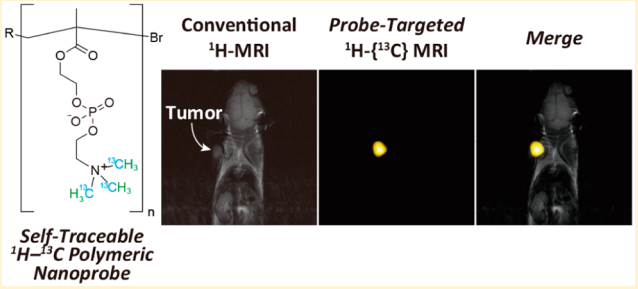

INTRODUCTION

Polymers are widely used in various delivery/localization events as drug carriers,[1,2] stabilizers of clinical protein and nucleic acid medications,[3,4] and lesion targeters. An obvious merit of polymers with an appropriate (>10 nm) size is that they escape from facile renal excretion.[5,6] The size has another significance in case of tumor targeting. Tumor tissues usually have defective endothelial cells with a wide opening and undeveloped lymphatic vessel, so that nanoparticles of the size range of 10−100 nm can permeate into the tumor and are retained therein. This is the so-called enhanced permeability and retention (EPR) effect.[7] Although the EPR effect has been widely utilized for passive tumor-targeting, its performance in

Received: October 12, 2014
Published: January 6, 2015

DOI: 10.1021/ja510479v
J. Am. Chem. Soc. 2015, 137, 799−806

terms of selectivity and efficiency is modest at best in most cases.[8] In addition, details of the EPR effect may still be far from fully elucidated. In this context, it is a pity that polymers are invisible and their direct pharmacokinetic analysis is usually very difficult. Invisibility of polymers may be one of obstacles to be overcome for their wide applications in diagnostic and therapeutic areas. We stepped toward the objective to visualize EPR polymers without using foreign labels such as fluorophores,[9,10] radioactive isotopes,[11] or paramagnetic contrast agents,[12] which may change the pharmacokinetics of the parent polymers.[11]

In this work, we focused on the applicability of multiple-resonance (heteronuclear-correlation) NMR to polymeric species and paid particular attention here to a zwitterionic phosphorylcholine moiety ($-OPO_3^-{-}CH_2CH_2{-}N^+(CH_3)_3$) as a repeating unit. Though phosphorylcholine polymers have recently received increasing attention,[13,14] we were also interested in the structural characteristics of this unit. Monomeric phosphorylcholine and its *n*-meric polymer possess, respectively, 9 and 9*n* (1800 for $n = 200$) equivalent methyl protons, which, upon enrichment of ^{13}C ($I = 1/2$) and ^{15}N ($I = 1/2$), are easily rendered unique (^{1}**H**$-^{13}C-^{15}N$) so as to be selectively and sensitively detected by double-resonance[15,16] or triple-resonance[17,18] NMR based on magnetic coherence transfer, $^1H \rightarrow {}^{13}C \rightarrow {}^1H$ (double) or $^1H \rightarrow {}^{13}C \rightarrow {}^{15}N \rightarrow {}^{13}C \rightarrow {}^1H$ (triple), upon successive excitation of the relevant nuclei. The selectivity factor (atom-based, probe/nonprobe) would be $1/0.011 = 91$ (double) or $1/(0.011 \times 0.0037) = 25\,000$ (triple), where 0.011 and 0.0037 are the natural abundance of ^{13}C and ^{15}N, respectively, and the sensitivity, which should be proportional to the number of respective protons (^{1}**H**$-^{13}C-^{15}N$), increases in proportion to the repetition number, that is, the degree of polymerization (*n*). Low selectivity and low sensitivity are the general weak points of NMR. With respect to the simultaneous improvement of these two key issues, synthetic polymers may be ideal targets of multiple-resonance NMR. Nevertheless, to the best of our knowledge multiple-resonance NMR (to say nothing of MRI) has not been applied to synthetic polymers. In the present work, we studied the pharmacokinetics of a $^{13}C/^{15}N$-enriched phosphorylcholine polymer (PMPC) as a self-reporting or self-traceable probe in tumor-bearing mice, where multiple-resonance NMR/MRI turned out to be remarkably useful for revealing several characteristics of this probe, not only as a highly selective tumor-targeter but also as a tumor-imager. The direct observation of size-dependence in the competition between renal excretion and tumor accumulation is another important point. The performance of polymers in delivery/localization processes, which has so far been only indirectly evaluated in most cases, may become directly evaluable by using self-traceable polymers in combination with multiple-resonance NMR/MRI.

RESULTS

$^{13}C/^{15}N$-enriched choline chloride ($HO-CH_2CH_2-{}^{15}N^+({}^{13}CH_3)_3\ Cl^-$) was converted by the phosphoramidite method into 2-methacryloyloxyethylphosphorylcholine ($^{13}C/^{15}N$-MPC, $M = 299$) (Supporting Information), which underwent atom transfer radical polymerization (ATRP)[19,20] with furan-protected maleimide bromide (R-Br) as an initiator by the Cu(I)Br/2,2′-bipyridine catalyst system to give $^{13}C/^{15}N$-enriched poly(2-methacryloyloxyethylphosphorylcholine), that is, $^{13}C/^{15}N$-PMPC, according to the scheme R-Br + *n*(MPC) → R-(MPC)$_n$-Br (Figure 1a). The $^{13}C/^{15}N$-PMPC used in this

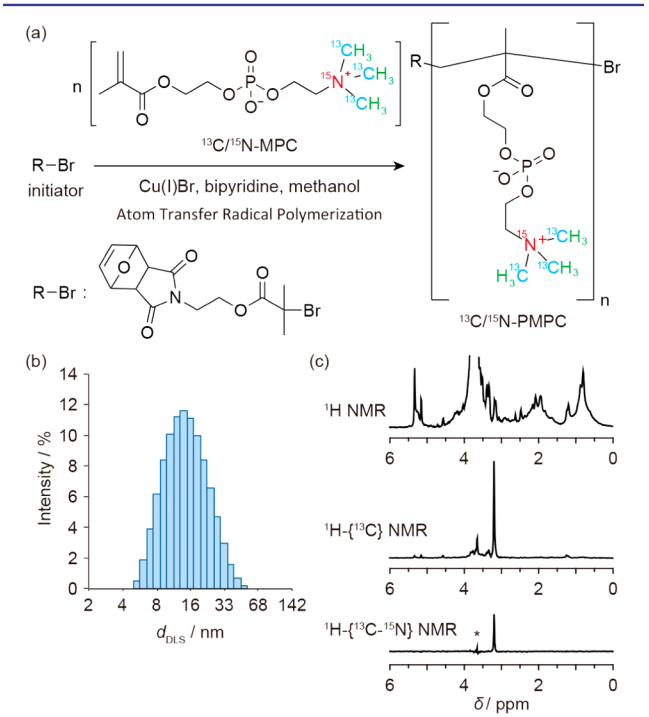

Figure 1. Preparation and properties of $^{13}C/^{15}N$-PMPC. (a) Polymerization of monomer $^{13}C/^{15}N$-MPC to afford polymer $^{13}C/^{15}N$-PMPC. (b) DLS analysis of $^{13}C/^{15}N$-PMPC$_{63000}$ (1 mg/mL) in water shows a mean hydrodynamic diameter of $d_{DLS} = 13.1 \pm 0.13$ nm ($n = 5$). (c) Conventional ^{1}H single-resonance (top), 1D ^{1}H−{^{13}C} double-resonance (middle), and 1D ^{1}H−{^{13}C−^{15}N} triple-resonance (bottom) NMR spectra of $^{13}C/^{15}N$-PMPC$_{63000}$ (1 μM) in 2 mM Tris−HCl/D_2O (pH 8.0) containing 0.1 mM EDTA and 0.1 mM 2-mercaptoethanol in the presence of a mouse liver lysate (10% v/v). The symbol * denotes a noise derived from the buffer solution (see also ref 18c).

study had a mean molecular weight of $M_n = 63\,000$ ($n = 210$), unless otherwise indicated, and a polydispersity index of $M_w/M_n = 1.6$. The $^{13}C/^{15}N$-PMPC$_{63000}$ polymer was independently shown by dynamic light scattering (DLS) to form nanoparticles with a mean hydrodynamic diameter of 13.1 ± 0.13 nm (Figure 1b) and a slightly negative surface potential (ζ) of -1.66 ± 0.45 mV. One-dimensional (1D) multiple-resonance NMR spectra of $^{13}C/^{15}N$-PMPC (1.0 μM), even in the presence of 10% mouse liver lysate, show a single, sharp resonance for the $^{15}N/^{13}C$-enriched methyl protons (^{1}**H**$-^{13}C-^{15}N$) at 3.18 ppm (Figure 1c). This figure shows how the overwhelming lysate-derived signals in conventional ^{1}H single-resonance (top) are mostly suppressed in ^{1}H−{^{13}C} double-resonance (middle), and several residual noise signals therein that arise from naturally occurring ^{1}H−^{13}C moieties in the lysate completely disappear in ^{1}H−{^{13}C−^{15}N} triple-resonance (bottom) (see the caption for the peak marked with * at $\delta \sim 3.7$ ppm). The mole-based sensitivity is in the nM range; signal-to-noise ratio (S/N) = 16.90 ± 0.27 (double-resonance, 16 scans taking ~1 min) or 6.94 ± 0.31 (triple-resonance, 16 scans taking ~1 min) for a 50 nM solution of the $^{13}C/^{15}N$-PMPC$_{63000}$ polymer ($50 \times 210 = 10\,500$ nM = 10.5 μM for the choline unit and $10.5 \times 9 = 94.5$ μM for ^{1}**H**$-^{13}C-^{15}N$ atoms). For the monomer $^{13}C/^{15}N$-MPC ($n = 1$), a similar sensitivity of S/N = 14.42 ±

DOI: 10.1021/ja510479v
J. Am. Chem. Soc. 2015, 137, 799−806

0.16 (double) or 9.92 ± 0.45 (triple) is attained only for a 10 μM (10 × 9 = 90 μM for ^{1}H−^{13}C−^{15}N atoms) solution under the same conditions; the increase in sensitivity for the polymer over the monomer is thus 10 μM/50 nM = 200. The sensitivity increases in proportion to the repetition number (n = 210) (Supporting Information Figure S6 for more details).

Preliminary MR images (Figure 2) were taken at 7T for four phantom samples: water as the ubiquitous "medium" of the

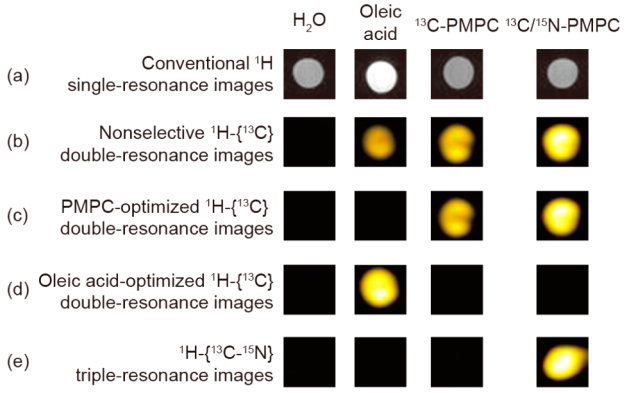

Figure 2. Magnetic resonance (MR) images of water, oleic acid (neat liquid with 1.1% natural abundance of ^{13}C), ^{13}C-PMPC (M_n = 35 000) in H_2O (0.23 mM = 8 mg/mL), and ^{13}C/^{15}N-PMPC (M_n = 44 000) in H_2O (0.18 mM = 8 mg/mL) in a test tube. (a) ^{1}H single-resonance MR images. (b) ^{1}H−{^{13}C} double-resonance MR images under nonselective conditions using block pulses. (c) ^{1}H−{^{13}C} double-resonance MR images under selective conditions using Gaussian-shaped pulses optimized for PMPC (δ_C = 55.0 ppm). (d) ^{1}H−{^{13}C} double-resonance MR images under selective conditions using Gaussian-shaped pulses optimized for oleic acid (δ_C = 30.0 ppm). (e) ^{1}H−{^{13}C−^{15}N} triple-resonance MR images. See the Supporting Information for details.

body, oleic acid (neat liquid with a 1.1% natural abundance of ^{13}C) as a model lipid, singly enriched ^{13}C-PMPC (M_n = 35 000; 8 mg/mL in H_2O, 0.23 mM), and doubly enriched ^{13}C/^{15}N-PMPC (M_n = 44 000; 8 mg/mL in H_2O, 0.18 mM). Data were acquired by the spin−echo (SE) or fast spin−echo (FSE) method following the double-[16a] or triple-resonance preparation[18c] in light of measured relaxation times (T_1 = 360 ms and T_2 = 183 ms for ^{1}H, T_1 = 512 ms and T_2 = 302 ms for ^{13}C, and T_1 = 14.1 s and T_2 = 8.27 s for ^{15}N for the ^{15}N/^{13}C methyl groups for the polymeric ^{13}C/^{15}N-PMPC probe).[21] ^{13}C nuclei in double-resonance imaging could be filtered by selective excitation using Gaussian-shaped pulses[22] with a half-bandwidth of 18 ppm (at 7T). Conventional ^{1}H-MRI gives positive images for all of the samples (Figure 2a). Although water is rendered completely MRI-silent (Figure 2b) under ^{1}H−{^{13}C} double-resonance conditions (SE; see Supporting Information Figure S8 for the FSE images), PMPC (δ_C = 55.0 ppm) and oleic acid (δ_C = 30.0 ppm) ($\Delta\delta$ = 25 ppm), which are both imageable upon nonselective excitation of the ^{13}C nuclei (Figure 2b), can be clearly distinguished upon selective excitation; PMPC is MRI-active under PMPC-optimized pulse conditions (Figure 2c) and vice versa under oleic acid-optimized pulse conditions (Figure 2d). The application of ^{1}H−{^{13}C−^{15}N} triple-resonance using the FSE method leads to the clear distinction of ^{13}C-PMPC (silent) and ^{13}C/^{15}N-PMPC (active) (Figure 2e), which are indistinguishable at the double-resonance level (Figure 2b and c). The detection limit of ^{13}C/^{15}N-PMPC$_{63000}$ lies at ∼10 μM under PMPC-optimized double-resonance and slightly higher than this but definitely lower than 90 μM under triple-resonance (Supporting Information Figure S7). These results indicate that double-resonance under probe-optimized conditions gives rise to satisfactory selectivity with respect to the exclusion of noise arising from natural-abundance ^{13}C-oleic acid as a model of lipids, which are major sources of noise in in vivo applications.

Ex vivo experiments using tumor-bearing mice inoculated with the mouse rectal cancer cell line (colon 26) at the right shoulder indicate that the present polymeric nanoprobe accumulates in the tumor with high selectivity, as revealed by a significant body of evidence. First, in the triple-resonance NMR spectra (Figure 3a; see Supporting Information Figure S12 for double-resonance spectra) of extracts of the tumor, liver, kidney, heart, and spleen removed at the day 2 time point

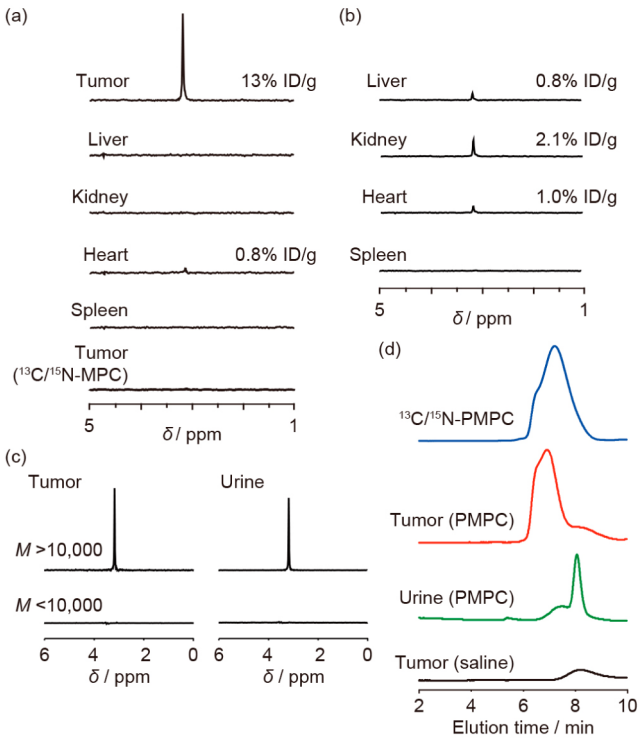

Figure 3. Behavior of ^{13}C/^{15}N-PMPC in tumor-bearing mice. (a) Triple-resonance NMR spectra for extracts of the tumor, liver, kidney, heart, and spleen of a tumor-bearing mouse (∼20 g) administered ^{13}C/^{15}N-PMPC$_{63000}$ (11.5 μmol/kg =730 mg/kg of body weight or 14.5 mg/mouse) or that of the tumor of a similar mouse administered monomer ^{13}C/^{15}N-MPC (2.4 mmol/kg =730 mg/kg of body weight or 14.5 mg/mouse) (bottom). The signal intensities are weight-normalized. The figures indicate quantified percent injected dose of the probe accumulated in the unit grams of tumor/organ. See Supporting Information Figure S12 for the double-resonance spectra. (b) Triple-resonance NMR spectra for extracts of the liver, kidney, heart, and spleen of a healthy mouse (∼20 g) administered ^{13}C/^{15}N-PMPC$_{63000}$ as in (a). (c) Triple-resonance spectra for the tumor extract (obtained as above) and urine collected after ultrafiltration. Top, nonfiltered, high molecular-weight (>10 000) residues of the tumor (left) and urine (right) samples. Bottom, filtered, low molecular-weight (<10 000) filtrates of the tumor (left) and urine (right) samples. (d) GPC profiles for the probe used, ^{13}C/^{15}N-PMPC$_{63000}$ (blue), nonfiltered tumor residue (red), and nonfiltered urine residue (green) obtained as above, and nonfiltered tumor residue of a mouse administered saline (black). The intensities are arbitrary unless otherwise indicated.[24]

DOI: 10.1021/ja510479v
J. Am. Chem. Soc. 2015, 137, 799−806

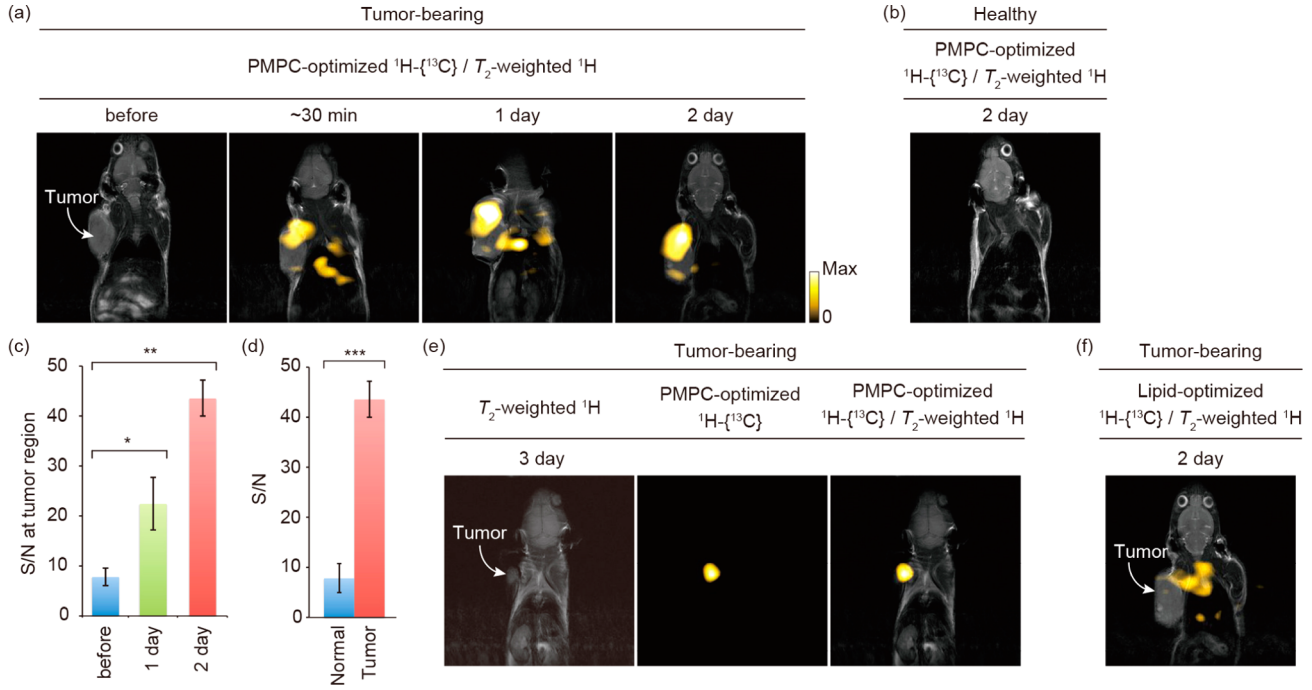

Figure 4. Probe-targeted MR images shown in yellow (FSE PMPC-optimized (unless otherwise indicated) double-resonance) overlaid on morphological images (T_2-weighted single-resonance) and accumulation of the probe in tumor tissue. (a) Time course of the change in merged images for a tumor-bearing mouse administered $^{13}C/^{15}N$-PMPC$_{63000}$ (11.5 μmol/kg = 730 mg/kg of body weight or 14.5 mg/mouse). (b) Merged image for a healthy mouse administered as in (a). (c) Time course of the change in the signal-to-noise ratios (S/N) at the tumor site for three tumor-bearing mice administered $^{13}C/^{15}N$-PMPC$_{63000}$ (4.6 μmol/kg = 290 mg/kg of body weight or 5.8 mg/mouse). (d) Comparison of S/N values at the day 2 time point at the tumor-bearing right shoulder and the normal left shoulder of three mice administered as in (c). (e) Merged image for a tumor-bearing mouse administered $^{13}C/^{15}N$-PMPC$_{63000}$ (1.5 μmol/kg = 100 mg/kg of body weight or 2.0 mg/mouse) and the constituent single-resonance and double-resonance images. (f) Merged (lipid-optimized double-resonance with single-resonance) image for a tumor-bearing mouse administered as in (a). Data in (c) and (d) represent mean ± SD *** $P < 0.001$. ** $P < 0.01$, * $P < 0.05$ (one-sided Student's t test). All images, normalized to preinjection of the probe, are set to the same or common yellow hot scale (0-max) of the ImageJ software, so that color intensities of panels a, b, and e can be directly compared with each other. See the Supporting Information for the field of view, matrix size, and other parameters.

from a tumor-bearing mouse administered $^{13}C/^{15}N$-PMPC$_{63000}$ (injected dose (ID) = 11.5 μmol/kg = 730 mg/kg of body weight or 14.5 mg/20 g of mouse), the methyl protons of the probe were detected highly selectively or almost exclusively in the tumor (2.9 mg, 20% ID or, when weight-normalized to the unit gram of the tumor, 13% ID/g), as well as in collected urine, and were just barely detected in the heart (0.8% ID/g) or only within the level of error in other normal organs. Indeed, there was no detectable accumulation of the probe in the liver, which is usually a major site for the deposition of tumor-targeting nanomedicines.[23] Second, the probe taken up by the tumor as well as excreted in urine retains a polymeric (>10 000) nature, as shown by molecular size fractionation with a 10 kDa cutoff molecular-weight filter (Figure 3c). More specifically, the gel permeation chromatography (GPC) profiles of the tumor (red) and urine (green) samples together with the probe used (blue), that is, $^{13}C/^{15}N$-PMPC$_{63000}$ (with a polydispersity index of 1.6 and a mean size of d_{DLS} = 13 nm with the size distribution profile shown in Figure 1b) clearly indicate that the fast-moving and hence larger (higher molecular-weight) portion of the probe is contained in the tumor (see footnote 24 for the tailing), whereas the slow-moving and hence smaller (lower molecular-weight) portion of the probe is excreted in urine (Figure 3d).[24] The polymeric nature is indeed essential; monomer $^{13}C/^{15}N$-MPC, in place of polymer $^{13}C/^{15}N$-PMPC, under otherwise identical conditions, did not accumulate in the tumor in any spectroscopically detectable (Figure 3a, bottom) or imageable amount (ex vivo, Supporting Information Figure S10, middle). These results, together with other evidence (Supporting Information Figure S9), suggest that, on one hand, the probe is remarkably stable against hydrolytic degradation and, on the other hand, is either captured and retained in the tumor or excreted in the urine in a molecular weight- and, hence, size-dependent manner. The amounts of the probe accumulated in the tumor (normalized to unit gram) increase with increasing ID's of the probe and are 0.86 mg/g (43% ID/g), 1.16 mg/g (20% ID/g), and 1.89 mg/g (13% ID/g) for ID = 2.0 mg, 5.8 mg, and 14.5 mg, respectively (see Quantification in Supporting Information for details). The local in-tumor concentration of the probe will be in the range of 13−30 μM, which is higher than the detection limit at around 10 μM (vide supra) of the PMPC-optimized double-resonance imaging.[25] The tumor must be imageable.

In vivo images of tumor-bearing and healthy mice were taken at 7T using the same machine as above under FSE (in most cases) probe-optimized double-resonance conditions without slice selection, as in the case of phantom samples (Figure 2); that is, they are projections through the body. Triple-resonance images turned out to be subject to noise due to body motion (see Supporting Information for details). In Figure 4, probe-targeted double-resonance MR images for tumor-bearing mice administered $^{13}C/^{15}N$-PMPC$_{63000}$ (1.5−11.5 μmol/kg = 100−730 mg/kg of body weight or 2.0−14.5 mg/20-g mouse) are shown in yellow overlaid on or merged with single-resonance tomographic (in-slice), morphological images. The two images were taken successively using the same machine for mice under

DOI: 10.1021/ja510479v
J. Am. Chem. Soc. 2015, 137, 799−806

anesthesia and hence the spatial error in their merging could be kept minimal. A typical time course of the change in merged (double/single) images is shown in Figure 4a (ID = 730 mg/kg of body weight or 14.5 mg/mouse). The probe, though distributed over a wide region including the tumor in 1 day,[26] is selectively localized in the tumor in 2−3 days. Quantitatively, the signal-to-noise ratios (S/N, where N refers to the standard deviation of noise at region outside of the mouse) at the tumor-bearing right shoulder for three independent mice (ID = 290 mg/kg of body weight or 5.8 mg/mouse) increase with time and reach 43.6 ± 3.6 at the day 2 time point (Figure 4c); S/N at the normal, contralateral left shoulder (7.8 ± 2.9) (Figure 4d) is only at the level for the PMPC-nonadministered tumor site (Figure 4c, before), the signal enhancement or tumor/normal contrast being $(S_{tumor} - S_{normal})/N = (S/N)_{tumor} - (S/N)_{normal}$ = 43.6−7.8 = 35.8. The lowest dose of the probe that can clearly visualize the tumor is 100 mg/kg of body weight, that is, 2.0 mg/20-g mouse (Figure 4e, S/N = 21.3). For comparison, the S/N at the tumor site of a mouse receiving the highest dose (730 mg/kg of body weight or 14.5 mg/mouse) of the probe (Figure 4a, 2 day) is 63.2. Thus, the S/N's of tumor image increase with increasing doses of the probe, in agreement with the analytical ex vivo results (vide supra). Selective excitation of the ^{13}C nuclei in the probe (δ_C = 55.0 ppm) is essential. Double-resonance under lipid-optimized pulse conditions (δ_C = 32.0 ppm) gives lipid images (Figure 4f)[27] that are quite different from those of the tumor (Figure 4a and e).

Control measurements indicate that probe-administered healthy mice (ID = 730 mg/kg of body weight or 14.5 mg/mouse) give no image under otherwise identical double-resonance conditions (Figure 4b). Ex vivo analysis of various organs removed from this healthy mouse shows that the probe is taken in a small but spectroscopically detectable amount in the liver (0.8% ID/g, ∼1.8 μM), kidney (2.1% ID/g, 4.8 μM), and heart (1.0% ID/g, 2.3 μM) (Figure 3b). However, the local concentrations of the probe in these organs, also shown in the parentheses, are slightly lower than the detection limit (∼10 μM) of double-resonance imaging, and hence, the probe even in healthy mice can not be imaged (Figure 4b).

Magnetic resonance spectroscopy (MRS) for a probe-administered mouse (ID = 4.6 μmol/kg = 290 mg/kg of body weight or 5.8 mg/mouse) indicated that ∼50% of the injected dose was rapidly lost (in urine) within 1 day after administration of the probe and ∼40% was retained in the body thereafter (Supporting Information Figure S13). The % ID values of the probe found in the tumor, urine collected for 2 days, and blood taken from a mouse treated as above and sacrificed 2 days after injection were 30%, 40%, and 13%, respectively. These values are consistent with the MRS results and confirm that ∼40% ID of the probe retained in the body is either accumulated in the tumor (30%) or circulates in the blood (13%).

DISCUSSION

NMR is considerably less sensitive than optical tools such as fluorescence. Furthermore, NMR imaging is several orders of magnitude less sensitive than spectroscopic NMR. This is why NMR can not be used as an effective tool for the pharmacokinetic analysis and visualization of molecular probes. On the other hand, the present PMPC probe of M_n = 63 000 has an intramolecularly 210-fold concentrated phosphorylcholine unit, which itself possesses nine equivalent marker methyl protons. Thus, it gives rise to outstanding (∼50 nM spectroscopic and ∼10 μM imaging under double-resonance conditions) sensitivities. In addition, the probe also shows remarkable selectivity. Noise that may arise from the natural-abundance $^1H-^{13}C$ moieties of endogenous components, particularly lipids, can be satisfactorily suppressed. This is because the methyl carbon bonded to the cationic ammonium center ($^1H-^{13}C-^{15}N^+$ in PMPC) exhibits a downfield-shifted chemical shift (δ_C = 55.0 ppm) that is sufficiently separated from that of lipid (δ_C = 32.0 ppm) to give a probe signal that is free from lipid noise under probe-optimized double-resonance conditions. It may also be important that the methyl groups bonded at the termini of pendant chains of a polymeric backbone supposedly possess good mobility and exhibit a sharp signal without noticeably undergoing relaxation-induced and sensitivity-lowering line broadening. The observed selectivity and sensitivity turned out to be sufficient to allow an unprecedented, direct, and unambiguous pharmacokinetic analysis of the present polymer, not only ex vivo but also in vivo (imaging). Indeed, the imaging sensitivity (∼10 μM) is sufficient to image the probe accumulated in the tumor (13−30 μM) but not so to image the probe taken by the liver or kidney even of healthy mice and by no means so to image endogenous ^{13}C-choline derivatives in tumor.[25] The clear imaging of tumor (Figure 4e) via an EPR tumor-targeter by itself has not been reported previously, although there are many new directions in MRI of tumors, which are based on either the labeling of tumor-targeters with paramagnetic contrast agents[28−30] or ^{19}F nuclei,[31,32] or the specific signal amplification of tumor-relevant molecules such as pyruvate or H_2O_2 (via the hyperpolarization of ^{13}C nuclei)[33] or glucose (via chemical exchange saturation transfer).[34] The high selectivity and sensitivity observed also suggest that the present method is applicable to a variety of synthetic polymers. In this context, it is important to note that double-resonance performs quite nicely here. This means that triple-resonance with doubly $^{13}C/^{15}N$-enriched probes is not necessarily required and singly ^{13}C-enriched probes should work when parameters such as chemical shifts and coupling constants are appropriate.

The most characteristic feature revealed for the present PMPC probe is its highly selective and highly efficient tumor-targeting with the percent ID up to 30% (see Quantification in Supporting Information for details). Coupled MRS (for a whole body) and ex vivo studies revealed the distribution of the probe at the day 2 time point, that is, 40−50% in excreted urine and ∼40% in the body (30% in tumor and 13% in blood). This suggests that the tumor is almost the sole deposition site for the in-body probe with an in-body percent ID as high as 30/(30 + 13) ≈ 70%. Such a gigantic number has never been precedented before. Size[23,35−37] and biocompatibility[38−40] are the most important factors that govern the pharmacokinetics of nanoparticles. Although smaller particles (<10 nm) undergo facile renal/urinary excretion[5,6] and larger ones (>100 nm) are cleared by the reticuloendothelial system (particularly through phagocytosis by macrophages distributed in various organs such as the liver),[41] intermediate particles (10−100 nm) have been claimed[23,35−37] to be subject to passive tumor-targeting by the so-called EPR effect, that is, size-allowed invasion of nanoparticles in tumor tissues via a wide opening of defective vascular wall and their retention therein owing to undeveloped lymphatic drainage.[7] The size-dependence of EPR has received considerable attention. An elaborate study indicated a maximal efficiency at ∼60 nm, and particles in the size range from

DOI: 10.1021/ja510479v
J. Am. Chem. Soc. 2015, 137, 799−806

several nanometers to >100 nm exhibited a broad size-efficiency profile.[42] Other investigators have suggested that the EPR effect was optimized for particles at ∼30 nm.[23] For smaller sizes, a recent study shows that ∼12 nm particles are still EPR-active.[37] The present results are consistent with this generalization in that (1) substantial proportions of the higher molecular-weight (larger size) and lower molecular-weight (smaller size) populations of the present probe $^{13}C/^{15}N$-$PMPC_{63000}$, with a mean size of ∼13 nm and a size distribution (5−70 nm) as shown in Figure 1b, undergo EPR accumulation in tumor and renal excretion, respectively, and (2) there is no appreciable macrophage/liver pathway, presumably because the size of the probes is controlled to be sub-100 nm.

The lack of spectroscopically detectable uptake of the probe by normal organs, especially the liver, of tumor-bearing mice (Figure 3a) may be at least partly explained in terms of tumor/liver competition for the probe overwhelmingly in favor of the tumor. This is because the probe is taken in a spectroscopically detectable amount in the liver (and kidney) of healthy mice (Figure 3b). However, the percent ID per gram remains only at a 1% level. The probe seems to have an intrinsic low affinity to the liver. A key player other than the size factor would be biocompatibility of the zwitterionic and, hence, neutral phosphorylcholine moiety, which constitutes the headgroup of cell membrane lipids. Particles that are surface-grafted with phosphorylcholine-containing polymers including PMPC are biologically inert.[13,14a] They are antibiofouling and prevent the adsorption of serum proteins.[13] They also escape from phagocytosis, probably because they are not recognized as foreign bodies by macrophages.[14a] This endows the probe with low toxicity (Supporting Information Figure S3) and good pharmacokinetic stability with respect to size and lifetime in the bloodstream, and stimulates the size-allowed passive EPR targeting of the probe to the tumor, which is slow but eventually efficient. The lowest clearly imageable dose of the probe (1.5 μmol/kg = 100 mg/kg or 2.0 mg/20-g mouse) is comparable to (on a weight basis) or even much lower than (on a molar basis) the clinical dose of Magnevist (0.1 mmol/kg = 74 mg/kg) used in traditional MRI. The percent ID (up to 30% ID) of the probe accumulated in the tumor may become higher upon more elaborate and narrower size-control of the probe in the EPR-relevant region. On the other hand, the size could be shifted to the more excretion-stimulating region. The critical size (at a mean size of around 13 nm) for the probe, which would separate facile renal excretion and stable retention in the tumor, and their respective size-dependencies (Figure 3d), thus, provide a basis for the elaborate design of polymeric EPR tumor-targeters.

CONCLUDING REMARKS

This work has opened a new area of MRI using molecular probes. Double- and triple-resonance techniques could also be applied in various MR schemes other than the spin−echo for a variety of polymers potentially in biological contexts. Polymers thus rendered self-traceable may provide a general tool to visualize various delivery/localization processes using them as carriers, stabilizers, or targeters. The efficiency of tumor-targeting may be further improved by modification of the probe, for example, with an active targeting ligand. Modification with a therapeutic unit may widen the applicability of self-traceable polymers. At the same time, the present work casts an important, yet-unsettled question: Why is tumor-targeting of the present PMPC probe so selective? Another issue to be addressed is clearance. The present probe is stably retained in the tumor for at least 1 week (Supporting Information Figure S13), although the long lifetime of the probe in the tumor might be a benefit if it is to be used as a carrier of antitumor drugs. With respect to triple-resonance, it failed to image the tumor due to body motion noise. Nevertheless, its remarkable selectivity may find its unique in vitro (e.g., perfect distinction of $^{1}H-^{13}C-^{14}N$ and $^{1}H-^{13}C-^{15}N$, Figures 2c and 2e) and in vivo (for motion-minimized domains) applications. Further work is now underway along these lines.

ASSOCIATED CONTENT

Supporting Information

(1) Experimental methods, (2) Preparation and cytotoxicity of $^{13}C/^{15}N$-PMPC, (3) Pulse sequences and evaluation of in vivo S/N ratios, (4) Sensitivities of multiple-resonance NMR and MRI, (5) In vivo behavior of $^{13}C/^{15}N$-PMPC, and (6) NMR spectra of enriched compounds. This material is available free of charge via the Internet at http://pubs.acs.org.

AUTHOR INFORMATION

Corresponding Authors

*teruyuki@scl.kyoto-u.ac.jp
*aoyama.yasuhiro.78z@st.kyoto-u.ac.jp

Author Contributions

#H.Y. and H.I. contributed equally.

Notes

The authors have a patent application (International application number: PCT/JP/2014/055848) on part of this work.

The authors declare no competing financial interest.

ACKNOWLEDGMENTS

This work was supported by the Innovative Techno-Hub for Integrated Medical Bio-Imaging of the Project for Developing Innovation Systems, from the Ministry of Education, Culture, Sports, Science and Technology (MEXT), Japan, and partly by Grant-in-Aid Nos. 25350977 and 23710268 from JSPS, Japan. T.K. acknowledges financial support from the Princess Takamatsu Cancer Research Fund and the Daiwa Securities Health Foundation. We thank Dr. Yuji Kamioka and Prof. Michiyuki Matsuda (Kyoto University) for their technical support with the animal experiments.

REFERENCES

(1) (a) Allen, T. M.; Cullis, P. R. *Science* **2004**, *303*, 1818−1822. (b) Harris, J. M.; Chess, R. B. *Nat. Rev. Drug Discovery* **2003**, *2*, 214−221. (c) Duncan, R. *Nat. Rev. Cancer* **2006**, *6*, 688−701. (d) Davis, M. E.; Chen, Z. G.; Shin, D. M. *Nat. Rev. Drug Discovery* **2008**, *7*, 771−782.

(2) (a) Joralemon, M. J.; McRae, S.; Emrick, T. *Chem. Commun.* **2010**, *46*, 1377−1393. (b) Larson, N.; Ghandehari, H. *Chem. Mater.* **2012**, *24*, 840−853.

(3) (a) Keefe, A. J.; Jiang, S. *Nat. Chem.* **2011**, *4*, 59−63. (b) Nguyen, T. H.; Kim, S.-H.; Decker, C. G.; Wong, D. Y.; Loo, J. A.; Maynard, H. D. *Nat. Chem.* **2013**, *5*, 221−227.

(4) (a) Putnam, D. *Nat. Mater.* **2006**, *5*, 439−451. (b) Park, T. G.; Jeong, J. H.; Kim, S. W. *Adv. Drug Delivery Rev.* **2006**, *58*, 467−486. (c) Keefe, A. D.; Pai, S.; Ellington, A. *Nat. Rev. Drug Discovery* **2010**, *9*, 537−550.

(5) Venturoli, D.; Rippe, B. *Am. J. Physiol. Renal Physiol.* **2005**, *288*, F605−F613.

DOI: 10.1021/ja510479v
J. Am. Chem. Soc. 2015, 137, 799−806

(6) Choi, H. S.; Liu, W.; Misra, P.; Tanaka, E.; Zimmer, J. P.; Itty Ipe, B.; Bawendi, M. G.; Frangioni, J. V. *Nat. Biotechnol.* **2007**, *25*, 1165−1170.
(7) Matsumura, Y.; Maeda, H. *Cancer Res.* **1986**, *46*, 6387−6392.
(8) Maeda, H.; Wu, J.; Sawa, T.; Matsumura, Y.; Hori, K. *J. Controlled Release* **2000**, *65*, 271−284.
(9) Hilderbrand, S. A.; Weissleder, R. *Curr. Opin. Chem. Biol.* **2010**, *14*, 71−79.
(10) (a) Ojida, A.; Honda, K.; Shinmi, D.; Kiyonaka, S.; Mori, Y.; Hamachi, I. *J. Am. Chem. Soc.* **2006**, *128*, 10452−10459. (b) Srikun, D.; Albers, A. E.; Nam, C. I.; Iavarone, A. T.; Chang, C. J. *J. Am. Chem. Soc.* **2010**, *132*, 4455−4465. (c) Komatsu, T.; Johnsson, K.; Okuno, H.; Bito, H.; Inoue, T.; Nagano, T.; Urano, Y. *J. Am. Chem. Soc.* **2011**, *133*, 6745−6751. (d) Wang, Y.; Zhou, K.; Huang, G.; Hensley, C.; Huang, X.; Ma, X.; Zhao, T.; Sumer, B. D.; DeBerardinis, R. J.; Gao, J. *Nat. Mater.* **2014**, *13*, 204−212.
(11) Cheng, T.-L.; Chuang, K.-H.; Chen, B.-M.; Roffler, S. R. *Bioconjugate Chem.* **2012**, *23*, 881−899 and references therein..
(12) For recent reviews on magnetic contrast agents, see, for example; (a) Na, H. B.; Song, I. C.; Hyeon, T. *Adv. Mater.* **2009**, *21*, 2133−2148. (b) Villaraza, A. J. L.; Bumb, A.; Brechbiel, M. W. *Chem. Rev.* **2010**, *110*, 2921−2959. (c) Terreno, E.; Castelli, D. D.; Viale, A.; Aime, S. *Chem. Rev.* **2010**, *110*, 3019−3042.
(13) Lewis, A. L. *Colloids Surf., B* **2000**, *18*, 261−275.
(14) (a) Moro, T.; Takatori, Y.; Ishihara, K.; Konno, T.; Takigawa, Y.; Matsushita, T.; Chung, U.-I.; Nakamura, K.; Kawaguchi, H. *Nat. Mater.* **2004**, *3*, 829−836. (b) Du, J.; Tang, Y.; Lewis, A. L.; Armes, S. P. *J. Am. Chem. Soc.* **2005**, *127*, 17982−17983. (c) Lewis, A.; Tang, Y.; Brocchini, S.; Choi, J.-W.; Godwin, A. *Bioconjugate Chem.* **2008**, *19*, 2144−2155. (d) Chen, X.; Parelkar, S. S.; Henchey, E.; Schneider, S.; Emrick, T. *Bioconjugate Chem.* **2012**, *23*, 1753−1763. (e) Soma, D.; Kitayama, J.; Konno, T.; Ishihara, K.; Yamada, J.; Kamei, T.; Ishigami, H.; Kaisaki, S.; Nagawa, H. *Cancer Sci.* **2009**, *100*, 1979−1985. (f) Madsen, J.; Canton, I.; Warren, N. J.; Themistou, E.; Blanazs, A.; Ustbas, B.; Tian, X.; Pearson, R.; Battaglia, G.; Lewis, A. L.; Armes, S. P. *J. Am. Chem. Soc.* **2013**, *135*, 14863−14870.
(15) Forseth, R. R.; Schroeder, F. C. *Curr. Opin. Chem. Biol.* **2011**, *15*, 38−47.
(16) (a) van Zijl, P. C. M.; Chesnick, A. S.; Despres, D.; Moonen, C. T. W.; Ruiz-Cabello, J.; van Gelderen, P. *Magn. Reson. Med.* **1993**, *30*, 544−551. (b) de Graaf, R. A.; Mason, G. F.; Patel, A. B.; Behar, K. L.; Rothman, D. L. *NMR Biomed.* **2003**, *16*, 339−357. (c) Kato, Y.; Okollie, B.; Artemov, D. *Magn. Res. Med.* **2006**, *55*, 755−761.
(17) (a) Wang, A. C.; Grzesiek, S.; Tschudin, R.; Lodi, P. J.; Bax, A. *J. Biomol. NMR* **1995**, *5*, 376−382. (b) Hutton, W. C.; Likos, J. J.; Gard, J. K.; Garbow, J. R. *J. Labelled Compd. Radiopharm.* **1998**, *41*, 87−95.
(18) (a) Yamaguchi, K.; Ueki, R.; Yamada, H.; Aoyama, Y.; Nonaka, H.; Sando, S. *Anal. Methods* **2011**, *3*, 1664−1666. (b) Ueki, R.; Yamaguchi, K.; Nonaka, H.; Sando, S. *J. Am. Chem. Soc.* **2012**, *134*, 12398−12401. (c) Yamada, H.; Mizusawa, K.; Igarashi, R.; Tochio, H.; Shirakawa, M.; Tabata, Y.; Kimura, Y.; Kondo, T.; Aoyama, Y.; Sando, S. *ACS Chem. Biol.* **2012**, *7*, 535−542.
(19) Matyjaszewski, K. *Macromolecules* **2012**, *45*, 4015−4039.
(20) Lobb, E. J.; Ma, I.; Billingham, N. C.; Armes, S. P.; Lewis, A. L. *J. Am. Chem. Soc.* **2001**, *123*, 7913−7914.
(21) For comparison, the relaxation times of ^{15}N-choline were reported to be T_1 = 285 ± 12 s and T_2 = 42 ± 3 s, see Gabellieri, C.; Reynolds, S.; Lavie, A.; Payne, G. S.; Leach, M. O.; Eykyn, T. R. *J. Am. Chem. Soc.* **2008**, *130*, 4598−4599.
(22) Bauer, C.; Freeman, R.; Frenkiel, T.; Keeler, J.; Shaka, A. J. *J. Magn. Reson.* **1984**, *58*, 442−457.
(23) Cabral, H.; Matsumoto, Y.; Mizuno, K.; Chen, Q.; Murakami, M.; Kimura, M.; Terada, Y.; Kano, M. R.; Miyazono, K.; Uesaka, M.; Nishiyama, N.; Kataoka, K. *Nat. Nanotechnol.* **2011**, *6*, 815−823.
(24) The black trace is for the tumor removed from a mouse administered saline in place of the probe. Although the intensities are arbitrary, those for the PMPC-administered and nonadministered tumor samples (red and black) are normalized to allow their direct comparison. In this context, the tailing in the tumor profile (red) in the low-molecular-weight region presumably arises from endogenous components of the tumor (black).
(25) The polymeric ^{13}C/^{15}N-PMPC$_{63000}$ probe is 210-mer (in average) of the choline monomer. The local concentration of the probe is (13 to 30) × 210 = 2700 to 6300 μM with respect to the monomeric choline. Tumors in mice are known to have high content of choline derivatives in the millimolar range, that is, naturally occurring ^{13}C-choline at the 0.01−0.1 mM = 10−100 μM level. This is much lower than that of the probe (2700−6300 μM) and is too low to be imaged, with the detection limit of the present double-resonance imaging being ∼10 μM for the polymer and, hence, 10 × 210 = 2100 μM for the ^{13}C-choline.
(26) In the triple-resonance NMR spectra of extracts of the tumor, liver, kidney, heart, and spleen as well as blood removed at the 30-min time point from a tumor-bearing mouse, the probe was detected most abundantly in the blood and also, in lesser amounts, in the tumor as well as various organs including the heart but not in the liver.
(27) This lipid image appears to be quite different from the tomographic (in-slice) lipid image obtained by the lipid-specified, conventional ^{1}H-MRI such as the Dixon method. (Dixon W. T. *Radiology* **1984**, *153*, 189−194). The present lipid-optimized double-resonance image is without slice selection, and hence, it is a projection through the body. In addition, it can target only the ^{1}H−^{13}C moieties with a 1.1% natural abundance of the lipids in marked contrast to the Dixon image that can target all of the ^{1}H−^{12}C moieties of the lipids. The former (double-resonance) may image only thick lipid regions. In Figure 4f, signal arises from the neck region, and the neck is well known to be rich in lipids.
(28) Huh, Y.-M.; Jun, Y.-W.; Song, H.-T.; Kim, S.; Choi, J.-S.; Lee, J.-H.; Yoon, S.; Kim, K.-S.; Shin, J.-S.; Suh, J.-S.; Cheon, J. *J. Am. Chem. Soc.* **2005**, *127*, 12387−12391.
(29) Kircher, M. F.; de la Zerda, A.; Jokerst, J. V.; Zavaleta, C. L.; Kempen, P. J.; Mittra, E.; Pitter, K.; Huang, R.; Campos, C.; Habte, F.; Sinclair, R.; Brennan, C. W.; Mellinghoff, I. K.; Holland, E. C.; Gambhir, S. S. *Nat. Med.* **2012**, *18*, 829−834.
(30) Olson, E. S.; Jiang, T.; Aguilera, T. A.; Nguyen, Q. T.; Ellies, L. G.; Scadeng, M.; Tsien, R. Y. *Proc. Natl. Acad. Sci. U.S.A.* **2010**, *107*, 4311−4316.
(31) Yu, J.-x.; Kodibagkar, V. D.; Cui, W.; Mason, R. P. *Curr. Med. Chem.* **2005**, *12*, 819−848.
(32) (a) Takaoka, Y.; Sakamoto, T.; Tsukiji, S.; Narazaki, M.; Matsuda, T.; Tochio, H.; Shirakawa, M.; Hamachi, I. *Nat. Chem.* **2009**, *1*, 557−561. (b) Thurecht, K. J.; Blakey, I.; Peng, H.; Squires, O.; Hsu, S.; Alexander, C.; Whittaker, A. K. *J. Am. Chem. Soc.* **2010**, *132*, 5336−5337. (c) Rolfe, B. E.; Blakey, I.; Squires, O.; Peng, H.; Boase, N. R. B.; Alexander, C.; Parsons, P. G.; Boyle, G. M.; Whittaker, A. K.; Thurecht, K. J. *J. Am. Chem. Soc.* **2014**, *136*, 2413−2419.
(33) (a) Day, S. E.; Kettunen, M. I.; Gallagher, F. A.; Hu, D.-E.; Lerche, M.; Wolber, J.; Golman, K.; Ardenkjaer-Larsen, J. H.; Brindle, K. M. *Nat. Med.* **2007**, *13*, 1382−1387. (b) Kennedy, B. W. C.; Kettunen, M. I.; Hu, D.-E.; Brindle, K. M. *J. Am. Chem. Soc.* **2012**, *134*, 4969−4977. (c) Nelson, S. J.; Kurhanewicz, J.; Vigneron, D. B.; Larson, P. E. Z.; Harzstark, A. L.; Ferrone, M.; van Criekinge, M.; Chang, J. W.; Bok, R.; Park, I.; Reed, G.; Carvajal, L.; Small, E. J.; Munster, P.; Weinberg, V. K.; Ardenkjaer-Larsen, J. H.; Chen, A. P.; Hurd, R. E.; Odegardstuen, L.-I.; Robb, F. J.; Tropp, J.; Murray, J. A. *Sci. Transl. Med.* **2013**, *5*, 198ra108. (d) Lippert, A. R.; Keshari, K. R.; Kurhanewicz, J.; Chang, C. J. *J. Am. Chem. Soc.* **2011**, *133*, 3776−3779.
(34) (a) Zhang, S.; Trokowski, R.; Sherry, A. D. *J. Am. Chem. Soc.* **2003**, *125*, 15288−15289. (b) Walker-Samuel, S.; Ramasawmy, R.; Torrealdea, F.; Rega, M.; Rajkumar, V.; Johnson, S. P.; Richardson, S.; Gonçalves, M. G. C.; Parkes, H. G.; Årstad, E.; Thomas, D. L.; Pedley, R. B.; Lythgoe, M. F.; Golay, X. *Nat. Med.* **2013**, *19*, 1067−1072.
(35) Fox, M. E.; Szoka, F. C.; Fréchet, J. M. J. *Acc. Chem. Res.* **2009**, *42*, 1141−1151.
(36) Petros, R. A.; DeSimone, J. M. *Nat. Rev. Drug Discovery* **2010**, *9*, 615−627.

DOI: 10.1021/ja510479v
J. Am. Chem. Soc. 2015, 137, 799−806

(37) Chauhan, V. P.; Stylianopoulos, T.; Martin, J. D.; Popović, Z.; Chen, O.; Kamoun, W. S.; Bawendi, M. G.; Fukumura, D.; Jain, R. K. *Nat. Nanotechnol.* **2012**, *7*, 383−388.
(38) Eldar-Boock, A.; Polyak, D.; Scomparin, A.; Satchi-Fainaro, R. *Curr. Opin. Biotechnol.* **2013**, *24*, 682−689.
(39) Jokerst, J. V.; Lobovkina, T.; Zare, R. N.; Gambhir, S. S. *Nanomedicine* **2011**, *6*, 715−728.
(40) Veronese, F. M.; Pasut, G. *Drug Discovery Today* **2005**, *10*, 1451−1458.
(41) Ilium, L.; Davis, S. S.; Wilson, C. G.; Thomas, N. W.; Frier, M.; Hardy, J. G. *Int. J. Pharm.* **1982**, *12*, 135−146.
(42) Tabata, Y.; Murakami, Y.; Ikada, Y. *J. Controlled Release* **1998**, *50*, 123−133.

DOI: 10.1021/ja510479v
J. Am. Chem. Soc. 2015, 137, 799−806